ASSESSMENT OF ALUMINUM ALLOY 6351 EGGSHELL REINFORCED COMPOSITE IN DRY TURNING USING RESPONSE SURFACE METHODOLOGY

Abstract

Lack of knowledge and comprehension of critical input parameters and material machinability has limited the industry's use of machining, making it challenging to meet requirements for machining responses and numerous other problems. This study uses response surface methods to evaluate Aluminum Alloy 6351 Eggshell Reinforced Composite as a turning machining material. The material removal rate (MRR), cutting force (F_c), and surface roughness (Ra) of the samples were examined. The mass percentage of the composite is 15% egg shell reinforcement and 85% aluminum alloy. Cutting force (Fc), surface roughness (Ra), and material removal rate (MRR) ANOVA tables show that several models have significant probability values (P-values) less than 0.05. Numerical optimization was used to identify combinations of process parameters that will give the best response of cutting force (Fc), surface roughness (Ra), and material removal rate (MRR). The Cutting force (Fc), surface roughness (Ra), and material removal rate (MRR) can all be predicted using the regression equation model that was created. The only input variable that significantly affects the cutting force is cutting speed.

The three-input variable studied has a significant effect on surface roughness (Ra) and material removal rate (MRR).

The optimization result obtained indicates that the optimal response for turning an aluminum alloy 6351 eggshell reinforced composite is 1.39676µm, 101.333N, and 2016.77mm3/min for surface roughness (Ra), cutting force (Fc), and material removal rate (MRR), respectively. This is achieved when the input variables of cutting speed (Vc), feed rate (Fr), and depth of cut (Dc), which are 589.479 rpm, 0.205976 mm/min, and 0.315524 mm, respectively, are used.

Keywords: *Numerical Optimization, Regression Equation, Material Removal Rate, Surface Roughness, Cutting Force.*

List of abbreviations

MRR	Material removal rate
AAERC	Aluminum alloy eggshell reinforced composite
AMMC	Aluminum metal matrix composites
BBD	Box-Behnken design
DOE	Design of experiment
Ra	Surface roughness
V_C	Cutting speed
F_C	Cutting force
D_C	Depth of cut
F_r	Feed rate

1. INTRODUCTION

CNC lathes have revolutionized the machining industry by automating turning processes. The computer numerical control lathe (CNC) is a type of machining tool that can be used to execute various operations on a workpiece. Among the several machining operations carried out by the CNC lathe, the most important operation is machine turning. Turning is one of the major machining techniques that is used to machine the outside diameter of a revolving cylindrical work piece [1, 2]. Rotating the work item till it reaches a pre-established size can help to decrease its diameter through turning process. In order to obtain the desired diameter and reduce the diameter, the work item is frequently turned [3, 4, 5]. Parts that are cylindrical are created during the turning process [6, 7]. Hence, it can be defined as the act of milling the outside of a work piece while it revolves in opposition to a cutting tool that is supplied perpendicular to the axis of the work piece.

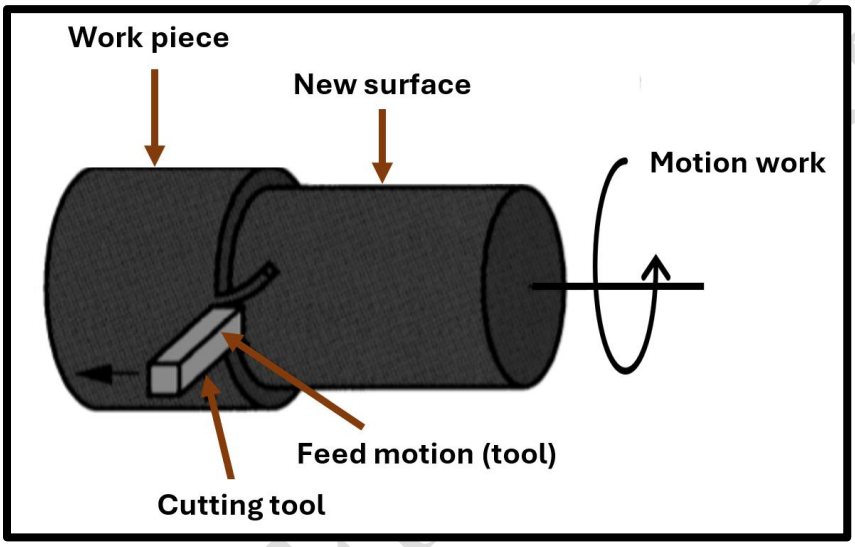

Fig. 1: turning operation concept [76]

The majority of operations requiring accuracy and surface smoothness use CNC. It is significant to note that the surface finish is impacted by the utilized operation speed [8-10]. V_C, D_C, and F_r being among the selected cutting parameters are utilized to create the expected response of MRR, F_C, and Ra [11-15]. The component's surface polish has been blamed for a variety of failures, some of which are catastrophic and cause enormous losses. In order to maximize the machining conditions and achieve a high surface polish, research has been developed for these reasons [16-22]. The measurement of a material's surface roughness is its micro-irregularities [23]. Many of a material's mechanical qualities, such as its capacity to withstand friction and wear, are predicted and determined by its surface roughness [16, 23-25]. When machining results in surface

specification variations, high surface integrity may not be produced by finishing [26, 27]. As a result, sufficient control measures must be taken to maintain surface roughness within allowable bounds, as this is a crucial criterion and technical prerequisite for assessing the quality of a product [28, 29]. The tool shape, tool material, cutting condition, and finishing of the tool are some of the aspects that actually determine surface roughness [16]. V_C, D_C, and F_r are three key machining characteristics that affects the machined Ra [15]. The measured volume of the material removed or the weight difference between the initial and post-machining states can be used to calculate the material removal rate which is the amount of material removed from the workpiece in a certain amount of time [30]. To guarantee the best possible machined output, the MRR idea must be taken into account when developing metal cutting techniques and selecting cutting instruments [31-34]. The force generated by the cutting tool as it slices the workpiece is known as the cutting force. Machining errors can result from issues with the equipment, process, and procedures used in metal machining [35-37]. The main issues with machining operations are the mistakes brought on by strong cutting force [38-41]. As a result, cutting force is now an essential factor to take into account to ensure a stable and effective machining operation [42-45].

Aluminum metal matrix composites (AMMC), are a valuable and quickly expanding material with strong mechanical and physical characteristics that make them ideal for a various technical application [46-52]. The exceptional mechanical and physical qualities of AMMC make them suitable materials for a wide range of applications [46-49, 53-57]. Reinforced metallic materials provide superior mechanical and chemical properties compared to ordinary engineering materials [58, 59]. Recently, interest has risen in creating composites using inexpensive and low-density reinforcements to achieve engineering aims and specific objectives [60-62]. Aluminum Matrix Composites (AMCs), having aluminum as a principal constituent, are a high performance, lightweight class of materials [7]. The reinforcement in AMCs can be continuous or discontinuous fibers, whiskers, or particles, with the highest significant dominant material [52, 63, 64]. Many composite materials used today are in line with applications needing the most outstanding levels of performance due to their performance, high availability, and affordability [65-67]. The matrix and reinforcement of the composite serve, respectively, to improve mechanical properties, facilitate load transmission, and ensure structural integrity [46-49, 53-55].

2 MATERIALS AND METHODS

2.1 MATERIALS

The materials and equipment utilized to do this task included a veneer caliper, measuring tape, Aluminum Alloy 6351, eggshell waste, a dynamometer (XXR-UN01), a surface tester (Mitutoyo sj-210), and a CNC lathe machine (250 PCD Boxford CNC lathe machine). Figure 2 to Figure 7, shows the Eggshells, Eggshell powder, Aluminum Alloy 6351 eggshell composite, Mutotuyo surface measuring instrument, mechanical stirrer with furnace and CNC lathe tool dynamometer respectively. Table 1 and Table 2 shows chemical compositions and the mechanical properties of the Aluminum alloy 6351, respectively.

Fig. 2: Egg shells

Fig. 3: Egg shell powder

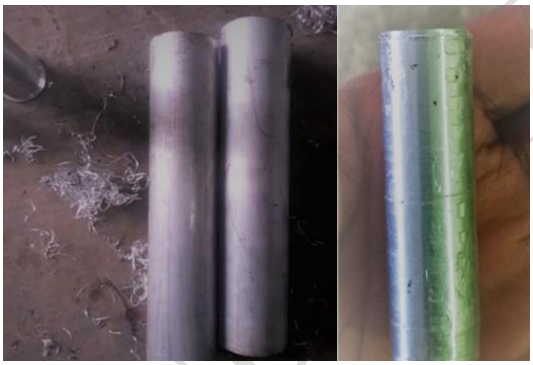

Fig. 4: Aluminum alloy 6351 eggshell composite

Fig. 5: Mutotuyo surface measuring instrument

Fig. 6: Mechanical Stirring with furnace

Fig. 7: CNC lathe tool dynamometer

Table 1: Composition of the A6351 alloy

Al	Si	Fe	Cu	Mn	Mg	Zn	Ti	V
Bal	7.0	0.1	0.002	0.006	0.4	0	0.13	0.02

Table 2: Mechanical properties of Al-6351 alloy

Sample	Specimen	Toughness (Joules)	Hardness (BHN)
1	Al-6351	6.638	60

2.2 METHODS

2.2.1 Aluminum Alloy 6351 eggshell reinforced composite preparation

The egg shells were collected and cleaned to remove the dust and particles after which they were washed thoroughly with water and allowed to dry in an oven heated to a temperature of 1000°C for a period of one hour. The desiccated egg shells were crushed and pulverized to room temperature to obtain the desired and finest crushed particle [68]. The resulting powder was passed through the necessary size sieves (>106 to <850 microns) to produce particles with a consistent size distribution. The composite composition by mass contained 85% Aluminum alloy and 15% Egg shell reinforcement [68]. The weights of the reinforcements (pulverized egg shell) were determined using electronic compact scale. The sourced Aluminum weight for the composite was determined using a weighing balance. The patterns used were made of wood while natural sand was used to prepare the sand mold.

Required amount of pulverized egg shell was kept in a furnace preheated in order to improve wettability [68]. A temperature probe was affixed to the aluminum to ensure total melting after the metal was heated to 700°C ± 50°C in a diesel-powered crucible furnace. After being heated to a temperature of around 600°C, the liquid aluminum was carefully deposited into the furnace to achieve a semi-solid condition [69]. To further increase the metal's wettability by lowering surface tension, raising surface energy, and lowering matrix reinforcement interface energy, magnesium powder (2%) was first added to the molten metal [70-73]. The heated, grounded egg shell particles were charged into the semi-solid melt at different temperatures and stirring intervals [68]. An automatic mechanical stirrer was used to stir the semi-solid composite mixture after it had been superheated to 750°C ± 50°C [68, 74, 75]. To create sound castings, the fluid was then put into a sand mold and let to set.

2.2.2 Design of experiment

The objective of the experimental design was to choose the machining settings for 15 runs using three levels and three components at random value combinations.

The goal of the studies was to find the ideal V_C, D_C, and F_r combination as input variables to generate the best possible MRR, F_C, and Ra. The desired experimental design's focal point was replicated three times in 15 runs using the Box-Behnken design (BBD) experimental design.

The machining process variables and their levels are given in Table 3.

Table 3: Independent process variable and design levels

Variables	Units	Low (-1)	Medium (0)	High (+1)
$\boldsymbol{V_C}$	Rpm	180	450	720
$\boldsymbol{F_r}$	mm/rev	0.2	0.3	0.4
$\boldsymbol{D_C}$	Mm	0.2	0.4	0.6

2.2.3 Experimental set up

Experiments on orthogonal turning was carried out on the 250 PCD Boxford CNC lathe machine multitasking machine tool at the University of Nigeria, LNG laboratory. The X, Y, and Z axes can all be linearly moved by the tool spindle. This arrangement made it simple to turn this machine and execute other tasks.

Cylindrical work piece of Aluminum Alloy 6351 eggshell composite of ∅220 mm diameter is fixed between the three jaws of the universal chuck. The three primary control variables chosen for this investigation are the V_C, D_C, and F_r. The performed experimental trials were carried out at various combinations of input variables (V_C, D_C, and F_r). For each trial, values for MRR, F_C, and Ra were accurately recorded. Ensuring the accuracy of the turning process model requires careful consideration of selected factors.

2.2.4 Cutting operation procedures

The first turning operation on the CNC lathe was used to cut the AAERC to the required diameter of 220 mm for each of the several samples.

AAERCs were turned to the required diameter of 220 mm for each of the samples using a CNC lathe. Process control parameters such as V_C, D_C, and F_r are combined to commence turning machining using DOE. Different machining settings are tested in order to obtain desired levels of MRR, F_C, and Ra. The chuck was fastened with the work material centered. The tool holder was secured with the HSS cutting insert, and the required adjustments were done.

F_C, and Ra were measured using a dynamometer and surface roughness tester (mitutoyo 2j-210) respectively. Figure 8 and Figure 9 shows the experimental setup and machined Aluminum Alloy 6351 reinforced composite respectively.

Fig. 8: Experimental setup (CNC lathe)

Fig. 9: Al. A6351 Eggshell machined sample

3 RESULTS AND DISCUSSION

This study explores the assessment of Aluminum Alloy 6351 eggshell reinforced composite as turning machining material using RSM**.** The impact of V_C, D_C, and F_r on the response were conducted on the material utilizing machining turning process. The design of experiment utilizes 3 level and 3 factors of box-Behnken design (BBD).

RSM combines statistical and mathematical techniques. Utilizing RSM to create continuous variable surfaces, assess response variables and interactions, and identify the optimal level range, this study examines the optimization of machining parameters of Aluminum Alloy 6351 eggshell reinforced composite.

A regression equation was fitted to describe the functional relationship between components and responses, and the optimal process parameters were ascertained by analyzing the regression equation, which was created using the DOE in a fair test by RSM. The second order of analytical process parameters was resolved by this method, which is the multivariate optimization.

Table 4 show the final data for the actual design after experiment conducted.

Table 4: Final data table of the actual design after experiment.

Runs	V_C	F_r	D_C	Ra	F_C	MRR
	(rpm)	(mm/min)	(mm)	(µm)	(N)	(mm^3/min)
1	180	0.2	0.4	1.16	171.2	2493.09
2	720	0.3	0.2	0.98	61.1	601.13
3	450	0.2	0.6	2.88	137.2	2488.45
4	720	0.2	0.4	2.12	95	1854.32
5	720	0.3	0.6	3.33	85.9	835.42
6	720	0.4	0.4	3.48	94.5	844.56
7	450	0.3	0.4	1.74	124.3	1516.4
8	450	0.4	0.2	1.14	119.7	735.8
9	180	0.3	0.6	2.9	169.7	1531.31
10	450	0.4	0.6	3.24	129.7	2352.69
11	450	0.3	0.4	1.38	130.2	1588.37
12	180	0.4	0.2	0.92	183.6	895.9
13	450	0.3	0.2	0.74	140	860.58
14	180	0.3	0.6	2.44	170.5	2237.11
15	450	0.2	0.2	0.9	115.3	1708.75

3.1 Quantitative assessment of F_C using ANOVA

Table 5 shows the analysis of variance of the F_C response to the Aluminum Alloy 6351 eggshell reinforced composite turning process. The model is considered significant with a P-value less than 0.00001 due to the study results demonstrating a non-significant lack of fit. The study indicates that V_C has a considerable impact on F_C during turning operations, as evidenced by the significant P-value of 0.0001. It is evident from the analysis of variance that this model is the most appropriate for response prediction because all mathematical models of F_C response have accuracy levels that surpass the 95% confidence threshold. Tables 5, 6, and 7, displays the F_C response variance analysis table. R-square, R-square (adj), and predicted R-square have respective values of 0.9529, 0.9176, and 0.8141. The precision of the accepted mathematical model is supported by the near proximity of all observed coefficients, R-sq, R-sq (adj), and predicted R-sq. The coefficient of determination, also known as the entity R-squared quantity, is further utilized to assess the RSM model's level of competency [54]. The generated mathematical model's adequacy is demonstrated by its R-squared values, which indicate how well the model fits the gathered data and how closely it approaches 1 [54].

Table 5: ANOVA table of F_C

Source	Sum of Squares	df	Mean Square	F-value	p-value	
Model	16617.38	6	2769.56	27.00	< 0.0001	significant
V_C	14891.61	1	14891.61	145.16	< 0.0001	
F_r	0.2560	1	0.2560	0.0025	0.9614	
D_C	160.28	1	160.28	1.56	0.2466	
$V_C \times F_r$	6.98	1	6.98	0.0681	0.8008	
$V_C \times D_C$	292.09	1	292.09	2.85	0.1300	
$F_r \times D_C$	43.39	1	43.39	0.4229	0.5337	
Residual	820.71	8	102.59			
Lack of Fit	802.99	6	133.83	15.10	0.0634	not significant
Pure Error	17.72	2	8.86			
Cor Total	17438.09	14				

Table 6: Fit statistics of F_C

Std. Dev.	10.13	**R²**	0.9529
Mean	128.53	**Adjusted R²**	0.9176
C.V. %	7.88	**Predicted R²**	0.8141
		Adeq. Precision	16.0680

Table 7: Coefficients in terms of coded factors of F_C

Factor	Coefficient Estimate	df	Standard Error	95% CI Low	95% CI High	VIF
Intercept	128.86	1	2.66	122.72	135.01	
V_C	-44.93	1	3.73	-53.53	-36.33	1.08
F_r	0.1838	1	3.68	-8.30	8.67	1.06
D_C	4.14	1	3.31	-3.50	11.78	1.07
$V_C \times F_r$	-1.39	1	5.34	-13.70	10.92	1.11
$V_C \times D_C$	8.27	1	4.90	-3.03	19.58	1.16
$F_r \times D_C$	-3.20	1	4.92	-14.55	8.15	1.16

Coded equation

$$\boldsymbol{F_C} = +128.86 - 44.93\, V_C + 0.1838\, F_r + 4.14\, D_C - 1.39\, V_C \times F_r + 8.27\, V_C \times D_C - 3.20\, F_r \times D_C \ldots\ldots\ldots (1)$$

F_C is predicted by entering the variables for V_C, D_C, and F_r into the equation that represents the coded equation of F_C. The procedure of comparing the factor coefficients of the components to ascertain their relative significance is made easier and more straightforward by the coded equation.

Actual equation

$$\boldsymbol{F_C} = +196.32061 - 0.212203\, V_C + 89.04748\, F_r - 0.221121\, D_C - (0.051575\, V_C \times F_r) + (0.153182\, V_C \times D_C) - (160.00341\, F_r \times D_C) \ldots\ldots\ldots (2)$$

The real parameters measured during the turning operation are V_C, D_C, and F_r for the actual equation. The coefficients show how the cutting force is impacted by each parameter and how those relationships work. When the real input values are available, the F_C can be predicted using the actual equation. These equations help in optimizing turning machining processes of the composite by predicting the F_C based on different parameter settings of V_C, D_C, and F_r.

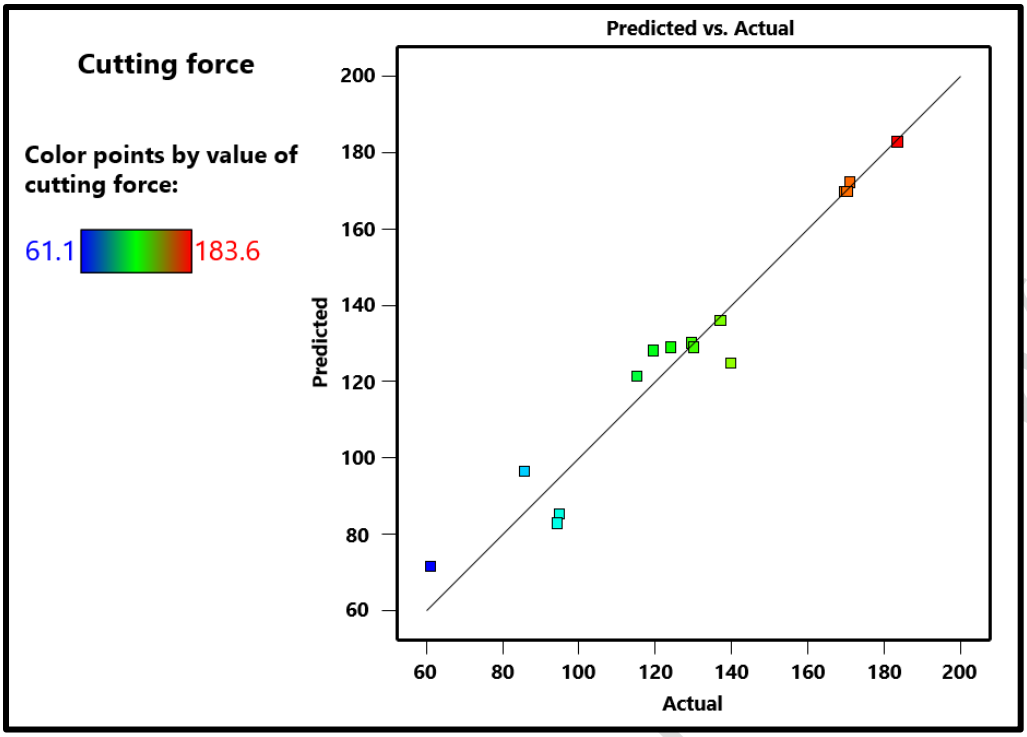

Fig. 10: Graph of predicted values and actual values of F_C.

Figure 10 shows the graph of F_C of predicted value against actual value. The figure shows a scattered plot comparing the predicted values versus actual values for the F_C. Each point represents a pair of actual and predicted values. The line, which displays the degree to which the expected and actual values agree, is indicated by the line connecting the points. The graph suggests that the model's predictions are quite accurate, as the points closely follow the line of best fit. Diagonal line represents perfect prediction, where predicted values match actual values exactly. Scatter Points shows color-coded based on the F_C, ranging from 61.1 (green) to 183.6 (red). The points are closely aligned with the diagonal line, indicating that the predictive model is quite accurate in estimating the F_C.

3.2 Quantitative assessment of MRR using ANOVA

Table 8 and Table 9 shows the analysis of variance and fit statistics table respectively. Table 8 demonstrates that the model is highly significant with a p-value of 0.0222, suggesting that the MRR is considerably influenced by the input variables (V_C, D_C, and F_r) taken into consideration. V_C, F_r and D_C are significant with a p-value of 0.0281, 0.0365 and 0.0070 respectively. The interactions of the input parameters like $F_r \times D_C$, $V_C \times F_r$ and $V_C \times D_C$ are not significant. However, the quadratic terms (${V_C}^2$, ${F_r}^2$, and ${D_C}^2$) are not significant. The lack of fit is not significant, suggesting that the model fits the data adequately. Table 9 displays the model's fit to the data as a result of R^2 obtaining a value of 0.9271. The coefficient of determination, also known as the entity R-squared quantity, is further utilized to assess the RSM model's competency. The difference between the R^2 of 0.9271 and the Adjusted R^2 of 0.7958 is less than 0.2, indicating a reasonable level of agreement. The match between the created model and the collected data is better when the R-square is nearer 1 [54]. The R-squared numbers demonstrate how well-developed the mathematical model is. There is an exceptional correlation between the independent variables, which is supported by the high values for all of the determination coefficients, which show that the modeling is highly significant. Table 10 shows that the MRR response mathematical models have accuracy levels in the analysis of variance that are greater than the 95% confidence level, suggesting that this model is the most suitable for response prediction.

Table 8: ANOVA table of MRR

Source	Sum of Squares	df	Mean Square	F-value	p-value	
Model	5.978E+06	9	6.643E+05	7.06	0.0222	significant
V_C	8.812E+05	1	8.812E+05	9.37	0.0281	
F_r	7.561E+05	1	7.561E+05	8.04	0.0365	
D_C	1.828E+06	1	1.828E+06	19.44	0.0070	
$V_C \times F_r$	54072.24	1	54072.24	0.5748	0.4825	
$V_C \times D_C$	1.436E+05	1	1.436E+05	1.53	0.2715	
$F_r \times D_C$	1.561E+05	1	1.561E+05	1.66	0.2540	
${V_C}^2$	3.141E+05	1	3.141E+05	3.34	0.1272	
${F_r}^2$	9.284E+05	1	9.284E+05	9.87	0.0256	
${D_C}^2$	1.795E+05	1	1.795E+05	1.91	0.2257	
Residual	4.703E+05	5	94063.88			
Lack of Fit	2.187E+05	3	72884.24	0.5792	0.6830	not significant
Pure Error	2.517E+05	2	1.258E+05			
Cor Total	6.449E+06	14				

Table 9: Fit statistics of MRR

Std. Dev.	306.70	**R^2**	0.9271
Mean	1502.93	**Adjusted R^2**	0.7958
C.V. %	20.41		

Table 10: Coefficients in terms of coded factors of MRR

Factor	Coefficient Estimate	df	Standard Error	95% CI Low	95% CI High	VIF
Intercept	1544.73	1	205.28	1017.04	2072.42	
V_C	-352.42	1	115.15	-648.41	-56.43	1.13
F_r	-326.05	1	115.00	-621.66	-30.43	1.12
D_C	454.72	1	103.14	189.59	719.85	1.13
$V_C \times F_r$	-129.97	1	171.42	-570.61	310.68	1.25
$V_C \times D_C$	-200.24	1	162.05	-616.80	216.33	1.38
$F_r \times D_C$	194.55	1	151.01	-193.64	582.75	1.20
${V_C}^2$	-302.26	1	165.41	-727.47	122.95	1.09
${F_r}^2$	545.40	1	173.60	99.14	991.66	1.20
${D_C}^2$	-257.79	1	186.62	-737.52	221.94	1.23

Coded equation

$$MRR = +1544.73 - 352.42\, V_C - 326.05\, F_r + 454.72\, D_C - 129.97\, V_C \times F_r - 200.24\, V_C \times D_C + 194.55\, F_r \times D_C - 302.26\, {V_C}^2 + 545.40\, {F_r}^2 - 257.79\, {D_C}^2 \ldots\ldots\ldots\ldots\ldots\ldots\ldots\ldots\ldots\ldots\ldots (3)$$

The coding equation of MRR can be anticipated by plugging in the values for V_C, F_r and D_C. The coded equation facilitates and simplifies the process of comparing the component factor coefficients to determine their respective importance. Regression models with coded coefficients show how each element affects the response. Coded equations show which way the response optimum is sharpest in the case of first-order models. It is less difficult to deal with varied scales and units for each element when coded factors are used. We are able to compare factors on a common scale by using the coded equation as a standardizing technique.

Actual equation

$$MRR = +5088.66895 + 5.35360\, V_C - 37709.43741\, F_r + 6179.75057\, D_C - 4.81359\, V_C \times F_r - 3.70806\, V_C \times D_C + 9727.61882\, F_r \times D_C - 0.004146\, {V_C}^2 + 54540.08488\, {F_r}^2 - 6444.76595\, {D_C}^2 \ldots\ldots\ldots\ldots\ldots\ldots\ldots\ldots\ldots\ldots\ldots\ldots\ldots\ldots (4)$$

The real parameters that are measured during the turning operation are V_C, F_r and D_C. The coefficients show how the various parameters and the MRR are correlated. When the actual input values are known, one can forecast the MRR using the actual equation. These formulas, which

take into account different V_C, F_r and D_C parameter values, can be used to anticipate the MRR for turning machining processes.

Simulation on how the response variable (output) and the actual factor levels relate to each other can be carried out using the actual equations. The response can be predicted for any given collection of factor values by fitting the model to the experimental data. When it comes to process optimization, this forecast aids in decision-making. The reaction can be maximized or minimized by using the actual formulae to determine the ideal factor choices. Techniques for optimization find the optimal factor levels by utilizing the equations. Strict formulas are necessary to attain the intended results. The impact of each factor is revealed by the coefficients in the real equations. While negative coefficients point to factors that may be reducing the response, positive coefficients show those that are increasing it.

The real equations aid in modifying factor concentrations to preserve intended response values. The formulas can be used to calculate what needs to be adjusted if the answer diverges from the intended outcome. We are able to measure how sensitive the response is to each element thanks to the real formulae. Robust process design is guided by sensitive information.

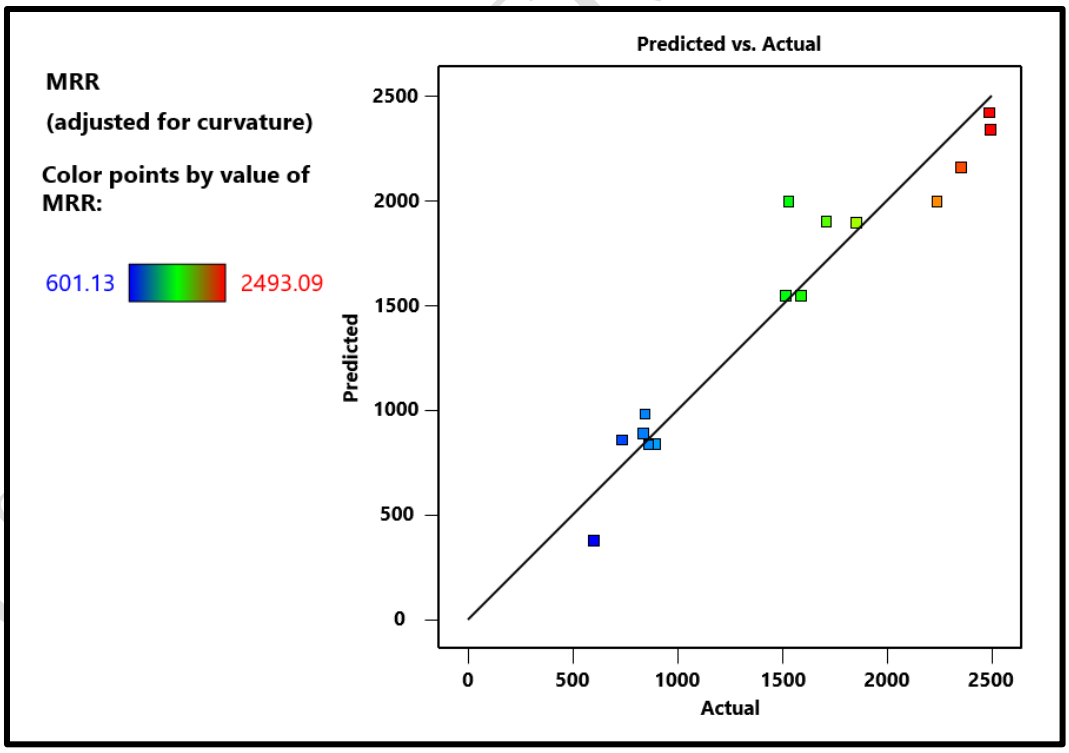

Fig. 11: Graph of predicted values and actual values of MRR.

Figure 11 shows the graph of MRR of predicted value against actual value. The MRR, which ranges from 601.13 (blue) to 2493.09 (red), is shown by a color gradient in the predicted vs. actual graph, which contrasts the predicted and actual values of a response variable. The diagonal line, which runs from lower left to upper right, shows the points in the data set where the anticipated and actual values exactly match. The accuracy of the predictions is indicated by the data points being dispersed about the diagonal line and better forecasts are shown by the points being closer to the line.

3.3 Quantitative assessment of Ra using ANOVA

Tables 11 and 12, respectively, present the fit statistics table and the analysis of variance table. The results presented indicate that the model has a p-value of less than 0.0001, indicating that V_C, F_r and D_C have a substantial impact on the Ra rate. V_C, F_r and D_C, all have significant p-values of 0.0001, 0.0188, and 0.0049, respectively. The model appears to have an appropriate fit to the data, since the lack of fit is not statistically significant. The fits statistic reveals an R^2 value of 0.9001, indicating a very good fit between the model and the data. There is a fair agreement as the gap between the predicted R^2 of 0.8152 and the adjusted R^2 of 0.8729 is less than 0.2.

The adequate precision of 16.095, which is greater than 4, indicates that the signal intensity is adequate. A statistically significant lack of fit is indicated by a 1.62 F-value. Table 13 demonstrates that the model is the most suitable for Ra prediction, with all mathematical models for Ra responses exhibiting accuracy levels in the analysis of variance exceeding the 95% confidence level.

Table 11: ANOVA table of Ra

Source	Sum of Squares	df	Mean Square	F-value	p-value	
Model	12.75	3	4.25	33.04	< 0.0001	significant
$\boldsymbol{V_C}$	1.58	1	1.58	12.30	0.0049	
$\boldsymbol{F_r}$	0.9751	1	0.9751	7.58	0.0188	
$\boldsymbol{D_C}$	11.60	1	11.60	90.21	< 0.0001	
Residual	1.41	11	0.1286			
Lack of Fit	1.24	9	0.1383	1.62	0.4391	not significant
Pure Error	0.1706	2	0.0853			
Cor Total	14.16	14				

Table 12: Fit statistics of Ra

Std. Dev.	0.3586	**R^2**	0.9001
Mean	1.96	**Adjusted R^2**	0.8729
C.V. %	18.33	**Predicted R^2**	0.8152
		Adeq. Precision	16.0947

Table 13: Coefficients in terms of coded factors of Ra

Factor	Coefficient Estimate	df	Standard Error	95% CI Low	95% CI High	VIF
Intercept	1.96	1	0.0926	1.75	2.16	
$\boldsymbol{V_C}$	0.4476	1	0.1276	0.1667	0.7285	1.01
$\boldsymbol{F_r}$	0.3514	1	0.1276	0.0705	0.6322	1.01
$\boldsymbol{D_C}$	1.09	1	0.1149	0.8381	1.34	1.03

Coded equation

$$Surface\ roughness\ (Ra) = +1.96 + 0.4476\,V_C + 0.3514\,F_r + 1.09\,D_C \ldots\ldots\ldots\ldots\ldots\ldots\ldots\ldots\ (5)$$

The coding equation of Ra can be anticipated by plugging in the values for V_C, F_r and D_C. The coded equation facilitates and simplifies the process of comparing the component factor coefficients to determine their respective importance. Regression models with coded coefficients show how each element affects the response. Coded equations show which way the response optimum is sharpest in the case of first-order models. It is less difficult to deal with varied scales and units for each element when coded factors are used. We are able to compare factors on a common scale by using the coded equation as a standardizing technique.

Actual equation

$$Surface\ roughness\ (Ra) = -2.02524 + 0.001658\,V_C + 3.51362\,F_r + 5.45449\,D_C \ldots\ldots\ldots (6)$$

The actual parameters that are measured in a turning process are the V_C, F_r and D_C. The correlation between the Ra and the different parameters is displayed by the coefficients. One can use the actual equation to forecast the Ra when the actual input values are known. The Ra for turning composite machining operations can be predicted using these formulas, which account for various V_C, F_r and D_C parameter values.

The actual equations can be used to simulate the relationship between the response variable (output) and the actual factor values. The model can be fitted to the experimental data to predict the response for any given set of factor values. This forecast helps with decision-making when it comes to process optimization. By figuring out the best factor selections using the actual equations, the response can be maximized or minimized. Equations are used by optimization techniques to determine the ideal factor levels. Tight formulations are required in order to achieve the desired outcomes. The coefficients in the actual equations show the effect of each element.

Positive coefficients indicate factors that are raising the reaction, while negative coefficients suggest those that might be decreasing it. To maintain the desired response values, factor concentrations can be changed with the use of the real equations. If the results deviate from what was planned, the formulas can be used to determine what has to be changed. The true equations allow us to quantify the response's sensitivity to each ingredient. Sensitive data serves as a roadmap for robust process design.

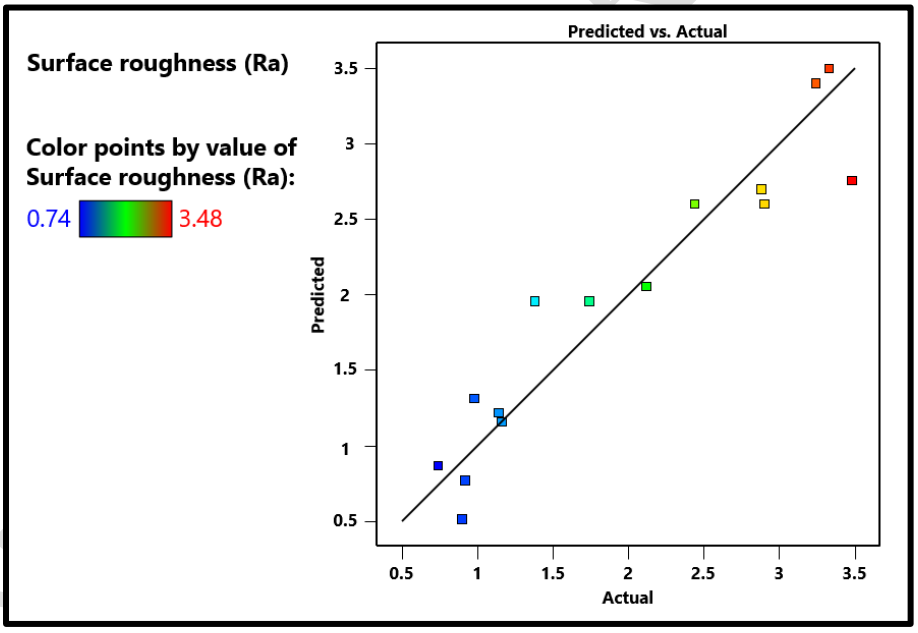

Fig. 12: Graph of predicted values and actual values of Ra.

Figure 12 shows the graph of Ra of predicted value against actual value. The Ra, which ranges from 0.74 (blue) to 3.48 (red), is shown by a color gradient in the predicted vs. actual graph, which contrasts the predicted and actual values of a response variable. The diagonal line, which runs from lower left to upper right, shows the points in the data set where the anticipated and actual values exactly match. The accuracy of the predictions is indicated by the data points being dispersed about the diagonal line and better forecasts are shown by the points being closer to the line.

3.4 Optimization using numerical method

Figure 13 shows the numerical optimization of Aluminum Alloy 6351 Eggshell Reinforced Composite. Desirability function optimization is the process of finding an arrangement of input variables that are then utilized to collectively optimize a set of answers by meeting the needs of each response in the set. Response optimization is the function's main objective. Optimizing sets typically involves two goals: reducing the response or increasing it. Additionally, each response's single expected value is represented by a weighted geometric mean. The optimization of desirability functions involves forecasting and refining the response to achieve the best possible combination of desired parameters. This function accepts the predicted values for every reaction meter on a preferred, or least ideal to most ideal, scale that runs from 0 to 1. The desired values for the expected composite are obtained by combining a single expected value. The best input variable setting is found by maximizing the integrated expectation value. The study utilizes the numerical optimization technique which provides clear explanation to generate the optimal input combination that will give the best response. The optimization carried out utilizes the desirability function of 1 which is the first out of 100 solutions.

The optimization result caried out shows that when the input variables of V_C, F_r and D_C of 589.479rpm, 0.205976mm/min, and 0.315524mm respectively are utilized in performing turning operation on Aluminum Alloy 6351 Eggshell Reinforced Composite, the optimal response is obtained with the values of Ra, F_C and MRR being 1.39676µm, 101.333N, and 2016.77mm^3/min, respectively.

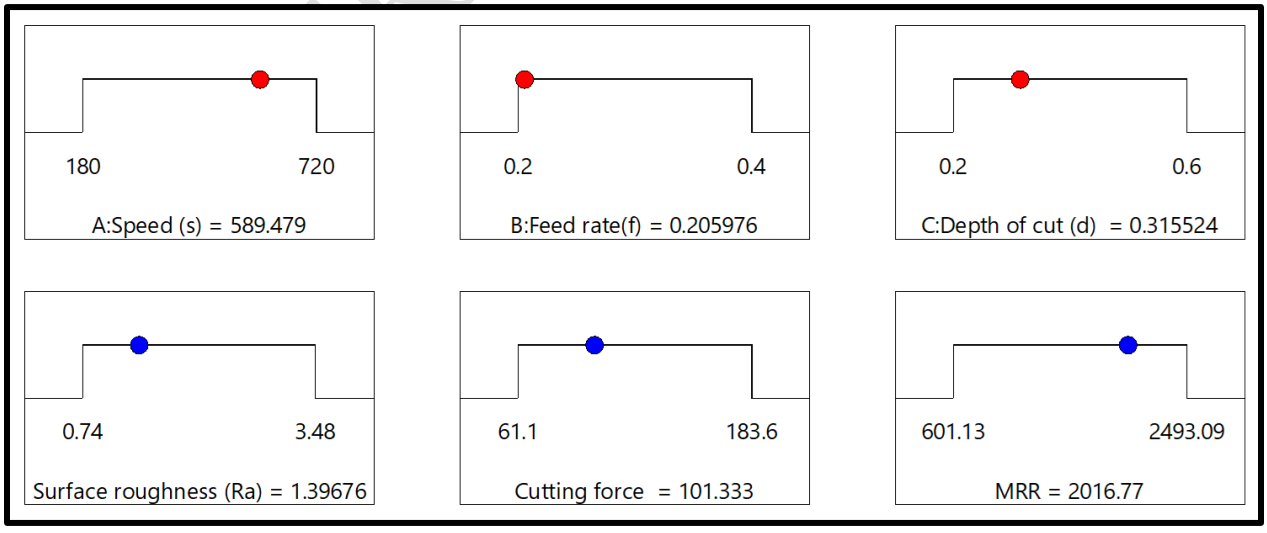

Fig. 13: Numerical optimization Aluminum Alloy 6351 Eggshell Reinforced Composite

4 CONCLUSIONS

This paper examines the assessment of Aluminum Alloy 6351 eggshell reinforced composite as turning machining material using response surface methodology. The samples were investigated for Ra, MRR and F_C. The conclusion drawn from the evaluated results were as follows:

1. Aluminum Alloy 6351 eggshell reinforced composite was successfully utilized for this investigation.
2. Numerical optimization was used to identify combinations of process parameters that will give the best response of F_C, Ra, and MRR.
3. The F_C, Ra, and MRR can all be predicted using the regression equation model that was created.
4. V_C is the only factor that has a significant effect on the F_C. The three-input variable studied has a significant effect on Ra and MRR.
5. The optimization result obtained indicates that the optimal response for turning an Aluminum Alloy 6351 eggshell reinforced composite is 1.39676µm, 101.333N, and 2016.77mm^3/min for Ra, F_C, and MRR, respectively. This is achieved when the input variables of V_C, F_r and D_C, which are 589.479 rpm, 0.205976 mm/min, and 0.315524 mm, respectively, are used.
6. The significance of this research is in its ability to furnish information regarding the appropriate input parameters that must be employed to get the desired output parameters. By adjusting these settings, you may reduce material waste, increase energy efficiency, and get the optimum surface finishing.

Disclaimer (Artificial intelligence)

Author(s) hereby declares that NO generative AI technologies such as Large Language Models (ChatGPT, COPILOT, etc.) and text-to-image generators have been used during writing or editing of manuscripts.

Competing interests

Authors have declared that no competing interests exist.

REFERENCES

[1] Vikram, K. A., Prasad, R. D. V., Lakshmi, V. V. K., & Praveen, A. M. V. (2023). Overview of turn-milling machining processes – A review. 020011. https://doi.org/10.1063/5.0182884.

[2] Yau, L. C., & Chockalingam, P. (2023). Material Removal Rate Study on Turning of Al Alloy. In Proceedings of the Multimedia University Engineering Conference (MECON 2022) (pp. 68–81). Atlantis Press International BV. https://doi.org/10.2991/978-94-6463-082-4_9.

[3] Butola, R., Sharma, V., Kanwar, S., Tyagi, L., Singari, R. M., & Tyagi, M. (2020). Optimizing the machining variables in CNC turning of aluminum-based hybrid metal matrix composites. SN Applied Sciences, 2(8), 1356. https://doi.org/10.1007/s42452-020-3155-8.

[4] Kumar, Dr. M. V. S., Kumar, Mr. M. P., Krishna, Mr. S. V., & Kumar, Mr. K. V. (2020). Optimization of CNC Turning Parameters in Machining EN19 using Face Centered Central Composite Design Based RSM. International Journal of Recent Technology and Engineering (IJRTE), 9(2), 889–896. https://doi.org/10.35940/ijrte.B3923.079220.

[5] Santhosh, A. J., Tura, A. D., Jiregna, I. T., Gemechu, W. F., Ashok, N., & Ponnusamy, M. (2021). Optimization of CNC turning parameters using face centred CCD approach in RSM and ANN-genetic algorithm for AISI 4340 alloy steel. Results in Engineering, 11, 100251. https://doi.org/10.1016/j.rineng.2021.100251.

[6] Gnanavelbabu, A., Arunachalam, V., Sunu Surendran, K. T., & Rajkumar, K. (2020). Optimization of machining parameters in CNC turning of AA6061-B4C-CNT hybrid composites using Grey-fuzzy method. IOP Conference Series: Materials Science and Engineering, 764(1), 012010. https://doi.org/10.1088/1757-899X/764/1/012010.

[7] Srinivasan, V., Kunjiappan, S., & Palanisamy, P. (2021). A brief review of carbon nanotube reinforced metal matrix composites for aerospace and defense applications. *International Nano Letters*, *11*(4), 321–345. https://doi.org/10.1007/s40089-021-00328-y.

[8] Akhtar, M. N., Sathish, T., Mohanavel, V., Afzal, A., Arul, K., Ravichandran, M., Rahim, I. A., Alhady, S. S. N., Bakar, E. A., & Saleh, B. (2021). Optimization of Process Parameters in CNC Turning of Aluminum 7075 Alloy Using L27 Array-Based Taguchi Method. Materials, 14(16), 4470. https://doi.org/10.3390/ma14164470.

[9] Nataraj, M., & Balasubramanian, K. (2017). Parametric optimization of CNC turning process for hybrid metal matrix composite. The International Journal of Advanced Manufacturing Technology, 93(1–4), 215–224. https://doi.org/10.1007/s00170-016-8780-4.

[10] Saini, P., & Singh, P. K. (2022). Characterization and optimization analysis on surface finish and energy consumption in turning of Al-4032/GMP MMC produced by stir casting. Proceedings of the Institution of Mechanical Engineers, Part C: Journal of Mechanical Engineering Science, 236(24), 11549–11563. https://doi.org/10.1177/09544062221110475.

[11] Arun Ramnath, R., Thyla, P., Mahendra Kumar, N., & Aravind, S. (2018). Optimization of machining parameters of composites using multi-attribute decision-making techniques: A review. Journal of Reinforced Plastics and Composites, 37(2), 77–89. https://doi.org/10.1177/0731684417732840.

[12] Gangwar, S., Mondal, S. C., Kumar, A., & Ghadai, R. K. (2024). Performance analysis and optimization of machining parameters using coated tungsten carbide cutting tool developed by novel S3P coating method. International Journal on Interactive Design and Manufacturing (IJIDeM). https://doi.org/10.1007/s12008-024-01852-9.

[13] Jamaludin, Z., Shamshol Ali, N. A., Rafan, N. A., & Abdullah, L. (2020). Effect of Cutting Forces on Surface Roughness for Varying Depth of Cut and Feed Rates in Milling Machining Process (pp. 195–203). https://doi.org/10.1007/978-981-13-9539-0_20.
[14] Rajendra, B., & Deepak, D. (2016). Optimization of Process Parameters for Increasing Material Removal Rate for Turning Al6061 Using S/N Ratio. Procedia Technology, 24, 399–405. https://doi.org/10.1016/j.protcy.2016.05.055.
[15] Tefera, A. G., Sinha, D. K., & Gupta, G. (2023). Experimental investigation and optimization of cutting parameters during dry turning process of copper alloy. Journal of Engineering and Applied Science, 70(1), 145. https://doi.org/10.1186/s44147-023-00314-5.
[16] Abellán-Nebot, J. V., Vila Pastor, C., & Siller, H. R. (2024). A Review of the Factors Influencing Surface Roughness in Machining and Their Impact on Sustainability. Sustainability, 16(5), 1917. https://doi.org/10.3390/su16051917.
[17] González, G., & Schulze, V. (2024). Surface conditioning in machining: optimizing component performance through advanced process modeling and control. Production Engineering, 18(2), 193–196. https://doi.org/10.1007/s11740-024-01268-0.
[18] Guleria, V., Kumar, V., & Singh, P. K. (2023). Recent Trends in the Amelioration and Prediction of Surface Roughness in Turning Process: A Bibliometric Analysis (pp. 77–90). https://doi.org/10.1007/978-981-19-4208-2_7.
[19] Kamguem, R., Djebara, A., & Songmene, V. (2013). Investigation on surface finish and metallic particle emission during machining of aluminum alloys using response surface methodology and desirability functions. The International Journal of Advanced Manufacturing Technology, 69(5–8), 1283–1298. https://doi.org/10.1007/s00170-013-5105-8.
[20] la Monaca, A., Murray, J. W., Liao, Z., Speidel, A., Robles-Linares, J. A., Axinte, D. A., Hardy, M. C., & Clare, A. T. (2021). Surface integrity in metal machining - Part II: Functional performance. International Journal of Machine Tools and Manufacture, 164, 103718. https://doi.org/10.1016/j.ijmachtools.2021.103718
[21] Micallef, C., Zhuk, Y., & Aria, A. I. (2020). Recent Progress in Precision Machining and Surface Finishing of Tungsten Carbide Hard Composite Coatings. Coatings, 10(8), 731. https://doi.org/10.3390/coatings10080731.
[22] Zeidler, H., Boettger-Hiller, F., Edelmann, J., & Schubert, A. (2016). Surface Finish Machining of Medical Parts Using Plasma Electrolytic Polishing. Procedia CIRP, 49, 83–87. https://doi.org/10.1016/j.procir.2015.07.038.
[23] Aghababaei, R., Brodsky, E. E., Molinari, J.-F., & Chandrasekar, S. (2022). How roughness emerges on natural and engineered surfaces. MRS Bulletin, 47(12), 1229–1236. https://doi.org/10.1557/s43577-022-00469-1.
[24] Bañón-García, F., Bermudo Gamboa, C., López-Fernández, J. A., Trujillo-Vilches, F. J., & Martín-Béjar, S. (2024). Correlation between Surface Texture, Wettability and Mechanical Strength of Polylactic Acid Parts Fabricated by Fused Filament Fabrication. Coatings, 14(8), 1033. https://doi.org/10.3390/coatings14081033.
[25] Magsipoc, E., Zhao, Q., & Grasselli, G. (2020). 2D and 3D Roughness Characterization. Rock Mechanics and Rock Engineering, 53(3), 1495–1519. https://doi.org/10.1007/s00603-019-01977-4.
[26] Pimenov, D. Y., Kiran, M., Khanna, N., Pintaude, G., Vasco, M. C., da Silva, L. R. R., & Giasin, K. (2023). Review of improvement of machinability and surface integrity in

machining on aluminum alloys. The International Journal of Advanced Manufacturing Technology, 129(11–12), 4743–4779. https://doi.org/10.1007/s00170-023-12630-4.
[27] Wu, D., Liu, S., & Wang, H. (2023). High surface integrity machining of typical aviation difficult-to-machine material blade. The International Journal of Advanced Manufacturing Technology, 129(7–8), 2861–2873. https://doi.org/10.1007/s00170-023-12533-4.
[28] Ružbarský, J. (2023). Roughness Control of Surfaces Using a Laser Profilometer with the Selected Material Cutting Technology. Materials, 16(11), 4109. https://doi.org/10.3390/ma16114109.
[29] Shao, M., Xu, D., Li, S., Zuo, X., Chen, C., Peng, G., Zhang, J., Wang, X., & Yang, Q. (2023). A review of surface roughness measurements based on laser speckle method. Journal of Iron and Steel Research International, 30(10), 1897–1915. https://doi.org/10.1007/s42243-023-00930-8.
[30] Liao, Z., la Monaca, A., Murray, J., Speidel, A., Ushmaev, D., Clare, A., Axinte, D., & M'Saoubi, R. (2021). Surface integrity in metal machining - Part I: Fundamentals of surface characteristics and formation mechanisms. International Journal of Machine Tools and Manufacture, 162, 103687. https://doi.org/10.1016/j.ijmachtools.2020.103687.
[31] Bilal, A., Perveen, A., Talamona, D., & Jahan, M. P. (2021). Understanding Material Removal Mechanism and Effects of Machining Parameters during EDM of Zirconia-Toughened Alumina Ceramic. Micromachines, 12(1). https://doi.org/10.3390/mi12010067.
[32] Cao, H., Zhou, K., & Chen, X. (2016). Stability-based selection of cutting parameters to increase material removal rate in high-speed machining process. Proceedings of the Institution of Mechanical Engineers, Part B: Journal of Engineering Manufacture, 230(2), 227–240. https://doi.org/10.1177/0954405415617931.
[33] Navaneethan, G., Palanisamy, S., Jayaraman, P. P., Kang, Y.-B., Stephens, G., Papageorgiou, A., & Navarro, J. (2024). A review of automated cutting tool selection methods. The International Journal of Advanced Manufacturing Technology, 133(3–4), 1063–1082. https://doi.org/10.1007/s00170-024-13823-1.
[34] Wang, B., Liu, Z., Cai, Y., Luo, X., Ma, H., Song, Q., & Xiong, Z. (2021). Advancements in material removal mechanism and surface integrity of high-speed metal cutting: A review. International Journal of Machine Tools and Manufacture, 166, 103744. https://doi.org/10.1016/j.ijmachtools.2021.103744.
[35] Astakhov, V. P. (2022). Cutting Force Modeling: Genesis, State of the Art, and Development (pp. 39–93). https://doi.org/10.1007/978-3-030-90487-6_2.
[36] Monroy Vazquez, K. P., Giardini, C., & Ceretti, E. (2014). Cutting Force Modeling. In CIRP Encyclopedia of Production Engineering (pp. 315–329). Springer Berlin Heidelberg. https://doi.org/10.1007/978-3-642-20617-7_6399.
[37] Monroy Vazquez, K. P., Giardini, C., & Ceretti, E. (2019). Cutting Force Modeling. In CIRP Encyclopedia of Production Engineering (pp. 417–432). Springer Berlin Heidelberg. https://doi.org/10.1007/978-3-662-53120-4_6399.
[38] Lee, S., Jo, W., Kim, H., Koo, J., & Kim, D. (2023). Deep learning-based cutting force prediction for machining process using monitoring data. Pattern Analysis and Applications, 26(3), 1013–1025. https://doi.org/10.1007/s10044-023-01143-1.
[39] Liu, M., Xie, H., Pan, W., Ding, S., & Li, G. (2023). Prediction of cutting force via machine learning: state of the art, challenges and potentials. Journal of Intelligent Manufacturing. https://doi.org/10.1007/s10845-023-02260-8.

[40] Radu, P., & Schnakovszky, C. (2024). A Review of Proposed Models for Cutting Force Prediction in Milling Parts with Low Rigidity. Machines, 12(2), 140. https://doi.org/10.3390/machines12020140.
[41] Yousefian, O., Balabokhin, A., & Tarbutton, J. (2020). Point-by-point prediction of cutting force in 3-axis CNC milling machines through voxel framework in digital manufacturing. Journal of Intelligent Manufacturing, 31(1), 215–226. https://doi.org/10.1007/s10845-018-1442-7.
[42] Charalampous, P. (2021). Prediction of Cutting Forces in Milling Using Machine Learning Algorithms and Finite Element Analysis. Journal of Materials Engineering and Performance, 30(3), 2002–2013. https://doi.org/10.1007/s11665-021-05507-8.
[43] Dubey, V., Sharma, A. K., Kumar, H., & Arora, P. K. (2022). Prediction of cutting forces in MQL turning of AISI 304 Steel using machine learning algorithm. Journal of Engineering Research. https://doi.org/10.36909/jer.ICMET.17177.
[44] Khlifi, H., Abdellaoui, L., & Bouzid Saï, W. (2024). Prediction of Cutting Force and Surface Roughness in Turning Using Machine Learning (pp. 213–222). https://doi.org/10.1007/978-3-031-42659-9_24.
[45] Sujuan, W., Tao, Z., Wenping, D., Zhanwen, S., & To, S. (2022). Analytical modeling and prediction of cutting forces in orthogonal turning: a review. The International Journal of Advanced Manufacturing Technology, 119(3–4), 1407–1434. https://doi.org/10.1007/s00170-021-08114-y.
[46] Kumar, A., Singh, V. P., Singh, R. C., Chaudhary, R., Kumar, D., & Mourad, A.-H. I. (2024). A review of aluminum metal matrix composites: fabrication route, reinforcements, microstructural, mechanical, and corrosion properties. Journal of Materials Science, 59(7), 2644–2711. https://doi.org/10.1007/s10853-024-09398-7.
[47] Pattar, J., Ramesh, D., Malghan, R. L., Kumar, A., Kumar, P., & H. M., V. (2024). Investigation of AA6063-based metal–matrix composites reinforced with TiO2 dispersoids through digitally assisted techniques for mechanical, tribological, and microstructural characterizations. Frontiers in Mechanical Engineering, 10. https://doi.org/10.3389/fmech.2024.1393959.
[48] Samuel Ratna Kumar, P. S., & Mashinini, P. M. (2022). Laser Additive Manufacturing of Aluminium Matrix Composites (pp. 73–90). https://doi.org/10.1007/978-3-030-89401-6_4.
[49] Wazeer, A., Mukherjee, A., Das, A., Sengupta, B., Mandal, G., & Sinha, A. (2024). Mechanical Properties of Aluminium Metal Matrix Composites: Advancements, Opportunities and Perspective (pp. 145–160). https://doi.org/10.1007/978-981-99-5982-2_9.
[50] Aynalem, G. F. (2020). Processing Methods and Mechanical Properties of Aluminium Matrix Composites. Advances in Materials Science and Engineering, 2020, 1–19. https://doi.org/10.1155/2020/3765791.
[51] Panchal, G. R., & Srinath, M. S. (2021). Development of Aluminum Matrix Composite Through Microwave Stir Casting (pp. 75–83). https://doi.org/10.1007/978-981-33-4018-3_7.
[52] Su, J., & Teng, J. (2021). Recent progress in graphene-reinforced aluminum matrix composites. *Frontiers of Materials Science, 15*(1), 79–97. https://doi.org/10.1007/s11706-021-0541-0.
[53] Laghari, R. A., Jamil, M., Laghari, A. A., Khan, A. M., Akhtar, S. S., & Mekid, S. (2023). A critical review on tool wear mechanism and surface integrity aspects of SiCp/Al MMCs

during turning: prospects and challenges. The International Journal of Advanced Manufacturing Technology, 126(7–8), 2825–2862. https://doi.org/10.1007/s00170-023-11178-7.

[54] Laghari, R. A., & Li, J. (2021). Modeling and optimization of cutting forces and effect of turning parameters on SiCp/Al 45% vs SiCp/Al 50% metal matrix composites: a comparative study. SN Applied Sciences, 3(7), 706. https://doi.org/10.1007/s42452-021-04689-z

[55] Li, J., & Laghari, R. A. (2019). A review on machining and optimization of particle-reinforced metal matrix composites. The International Journal of Advanced Manufacturing Technology, 100(9–12), 2929–2943. https://doi.org/10.1007/s00170-018-2837-5.

[56] Wong, W. L. E., & Seetharaman, S. (2021). Metal Matrix Composites (pp. 129–158). https://doi.org/10.1007/978-3-030-71438-3_6.

[57] Zhou, J., Li, C.-J., & Li, C.-X. (2020). Fabrication of Metal Matrix Composites via High-Speed Particle Implantation. *Journal of Thermal Spray Technology*, *29*(8), 1910–1925. https://doi.org/10.1007/s11666-020-01106-6.

[58] Manjunath, R., Kumar, D., & Kumar, A. (2021). A Review on the Significance of Hybrid Particulate Reinforcements on the Mechanical and Tribological Properties of Stir-Casted Aluminum Metal Matrix Composites. *Journal of Bio- and Tribo-Corrosion*, *7*(3), 122. https://doi.org/10.1007/s40735-021-00558-9.

[59] Srivastava, A. (2017). Recent Advances in Metal Matrix Composites (MMCs): A Review. Biomedical, *Journal of Scientific & Technical Research*, *1*(2). https://doi.org/10.26717/BJSTR.2017.01.000236.

[60] Abdur Rahman, M., Haque, S., Athikesavan, M. M., & Kamaludeen, M. B. (2023). A review of environmentally friendly green composites: production methods, current progresses, and challenges. *Environmental Science and Pollution Research*, *30*(7), 16905–16929. https://doi.org/10.1007/s11356-022-24879-5.

[61] Crupi, V., Epasto, G., Napolitano, F., Palomba, G., Papa, I., & Russo, P. (2023). Green Composites for Maritime Engineering: A Review. *Journal of Marine Science and Engineering*, *11*(3), 599. https://doi.org/10.3390/jmse11030599.

[62] Liu, S., Liu, L., Yang, K., Yuan, Z., Li, X., Li, C., & Meng, S. (2023). Reinforcing the mechanical properties of bamboo fiber/low density polyethylene composites with modified bamboo-woven structure. Journal of Materials Science, 58(25), 10359–10369. https://doi.org/10.1007/s10853-023-08682-2.

[63] Barot, R. P., Desai, R. P., & Sutaria, M. P. (2023). Recycling of Aluminium Matrix Composites (AMCs): A Review and the Way Forward. *International Journal of Metal casting*, *17*(3), 1899–1916. https://doi.org/10.1007/s40962-022-00905-7.

[64] Mistry, J. M., & Gohil, P. P. (2018). Research review of diversified reinforcement on aluminum metal matrix composites: fabrication processes and mechanical characterization. *Science and Engineering of Composite Materials*, *25*(4), 633–647. https://doi.org/10.1515/secm-2016-0278.

[65] Asyraf, M. R. M., Ilyas, R. A., Sapuan, S. M., Harussani, M. M., Hariz, H. M., Aiman, J. M., Baitaba, D. M., Sanjay, M. R., Ishak, M. R., Norkhairunnisa, M., Sharma, S., Alam, M. A., & Asrofi, M. (2022). Advanced Composite in Aerospace Applications: Opportunities, Challenges, and Future Perspective. *In Advanced Composites in Aerospace Engineering Applications*, 471–498. Springer International Publishing. https://doi.org/10.1007/978-3-030-88192-4_24.

[66] Oladele, I. O., Omotosho, T. F., & Adediran, A. A. (2020). Polymer-Based Composites: An Indispensable Material for Present and Future Applications. *International Journal of Polymer Science*, 2020, 1–12. https://doi.org/10.1155/2020/8834518.
[67] Sanjay, M. R., Arpitha, G. R., Naik, L. L., Gopalakrishna, K., & Yogesha, B. (2016). Applications of Natural Fibers and Its Composites: An Overview. Natural Resources, 07(03), 108–114. https://doi.org/10.4236/nr.2016.73011.
[68] Nwobi-Okoye, C. C., & Uzochukwu, C. U. (2020). RSM and ANN modeling for production of Al 6351/ egg shell reinforced composite: Multi objective optimization using genetic algorithm. Materials Today Communications, 22, 100674. https://doi.org/10.1016/j.mtcomm.2019.100674.
[69] Pola, A., Tocci, M., & Kapranos, P. (2018). Microstructure and Properties of Semi-Solid Aluminum Alloys: A Literature Review. Metals, 8(3), 181. https://doi.org/10.3390/met8030181.
[70] Chen, L., & Yao, Y. (2014). Processing, Microstructures, and Mechanical Properties of Magnesium Matrix Composites: A Review. Acta Metallurgica Sinica (English Letters), 27(5), 762–774. https://doi.org/10.1007/s40195-014-0161-0.
[71] Malaki, M., Fadaei Tehrani, A., Niroumand, B., & Gupta, M. (2021). Wettability in Metal Matrix Composites. Metals, 11(7), 1034. https://doi.org/10.3390/met11071034.
[72] Razzaq, A. M., Abdul Majid, D. L. A., Ishak, M. R., & M. B, U. (2017). A Brief Research Review for Improvement Methods the Wettability between Ceramic Reinforcement Particulate and Aluminium Matrix Composites. IOP Conference Series: Materials Science and Engineering, 203, 012002. https://doi.org/10.1088/1757-899X/203/1/012002.
[73] Ren, J.-Y., Ji, G.-C., Guo, H.-R., Zhou, Y.-M., Tan, X., Zheng, W.-F., Xing, Q., Zhang, J.-Y., Sun, J.-R., Yang, H.-Y., Qiu, F., & Jiang, Q.-C. (2024). Nano-Enhanced Phase Reinforced Magnesium Matrix Composites: A Review of the Matrix, Reinforcement, Interface Design, Properties and Potential Applications. Materials, 17(10), 2454. https://doi.org/10.3390/ma17102454.
[74] Mishra, D., & Tulasi, T. (2020). Experimental Investigation on Stir Casting Processing and Properties of Al 6082/SiC Metal Matrix Composites (pp. 159–168). https://doi.org/10.1007/978-981-15-1124-0_14.
[75] Singh, A. K., Soni, S., & Rana, R. S. (2022). Recent Trends on Furnace Design and Stirrer Blade Geometry Used in Stir Caster: A Focused Review (pp. 147–159). https://doi.org/10.1007/978-981-16-5371-1_14.
[76] Abdallah, A. (2014). Optimization of cutting parameters for surface roughness in CNC turning machining with aluminum alloy 6061 material. IOSR Journal of Engineering, 4(10), 01–10. https://doi.org/10.9790/3021-041010110.

.